Detection of the chirality of twisted bilayer graphene by the optical absorption

Xin-Miao Qiu,[1] Ning Yang,[2,3] Weidong Chu,[2,3] and Jie-Yun Yan[1,4,*]

[1]*School of Science, Beijing University of Posts and Telecommunications, Beijing 100876, China*
[2]*Institute of Applied Physics and Computational Mathematics, Beijing 100088, China*
[3]*National Key Laboratory of Computational Physics, Beijing 100088, China*
[4]*State Key Laboratory of Information Photonics and Optical Communications, Beijing University of Posts and Telecommunications, Beijing 100876, China*

(Received 27 November 2023; revised 7 January 2024; accepted 4 March 2024; published 18 March 2024)

Twisted bilayer graphene possesses intrinsic chirality, which has received less attention among the extensive research conducted on twistronics. In this paper, the optical absorption theory beyond the common linear perturbation is developed with more sophisticated light-electron interactions considered. Numerical calculations based on the theory found that reducing the twisted angle produces a redshift of absorption in the high-frequency range, while increasing absorption strength in the low-frequency domain, which can be further significantly enhanced when applying an interlayer bias. More importantly, the absorption spectroscopy is shown to be an effective way to detect both the chirality and the anisotropy of the twisted bilayer structure.

DOI: 10.1103/PhysRevB.109.125419

I. INTRODUCTION

Recently, there has been increasing research interest in few-layer two-dimensional materials, particularly those with a twisted angle between them [1–7]. Such twisted metasurfaces can give rise to a moiré pattern, introducing another spatial period for electrons. The twisted angle, as a new degree of freedom, allows for flexible manipulation of electronic properties without altering the material, because the electrons behave with a strong dependence on the stacking arrangement. For example, a transition from a Fermi liquid to a strongly correlated system has been observed in magic angle twisted bilayer graphene (TBG) [8], which exhibits unique properties including superconductivity [9], interaction-driven insulators [10], orbital magnets [11], etc. Moreover, twisted bilayer graphene and its derived systems provide ideal platforms for exploring arbitrary and fractional Chern numbers due to its tunable band structure and geometry [12–15]. A low-energy continuum model Hamiltonian is constructed by assuming that the small Brillouin zone in a small twisted angle ($\lesssim 10^\circ$) TBG system can be filled with wave vectors near the Dirac point of the two graphene layers. Bistritzer and MacDonald's work [16] accurately predicts the presence of a flat-band structure at the magic twisted angle (1.05°), which serves as a fundamental approach for investigating strongly correlated TBG systems at small twisted angles. Subsequently, twistronics, a technique that involves manipulating the relative twisted angle between successive layers in a two-dimensional material to control its electronic properties, has garnered significant attention.

In this kind of system, a helical structure is formed due to the twisting. In other words, the twisting of the upper layer in both clockwise and counterclockwise directions relative to the bottom layer imparts chirality to the bilayer material. Chirality holds significant importance and potential applications, particularly in biochemistry [17], the chiral sensing [18,19], and chiral catalysis [20,21], among others. The optical method is supposed to be an effective way to study the chirality and has been realized in experiment [22]. Since then, many theoretical methods have been developed to understand the optical response in theory. However, the traditional method, dynamical conductivity [23–27], does not adequately consider the response to light polarization (including linear and circular polarization). Additionally, the continuum model [16] is accurate only for small-angle twisted situations and is not applicable to TBG systems with a large twisted angle. The ellipticity in optical absorption in such a system was studied by some researchers mainly through the photoconductivity formula [28–32]. These works manifest the effect of chirality in each way as taking into account the propagation of light in the perpendicular direction, but their models are based on various approximations or simplifications on the interlayer interaction or in-plane response. A microscopic theory considering the electrons' all possible hoppings in a detailed lattice is still absent. Moreover, the ellipticity can only be ascertained when at least second-order light-matter interactions are included, on which level the contribution from the magnetic component of light cannot be neglected.

In this paper, we investigate the optical absorption properties of TBG and manage to detect its chirality through the optical method based on a microscopic model. We develop a more advanced theory of optical absorption that goes beyond linear light-induced perturbation. This theory considers the higher-order light-TBG interactions and provides a comprehensive understanding of the system's response to optical polarization, including both linear and circular cases. To validate the theory, we perform numerical calculations, which demonstrate the effectiveness of the optical method in identifying the chirality of TBG as well as anisotropy. More interestingly, we also confirm the significantly increased

*Corresponding author: jyyan@bupt.edu.cn

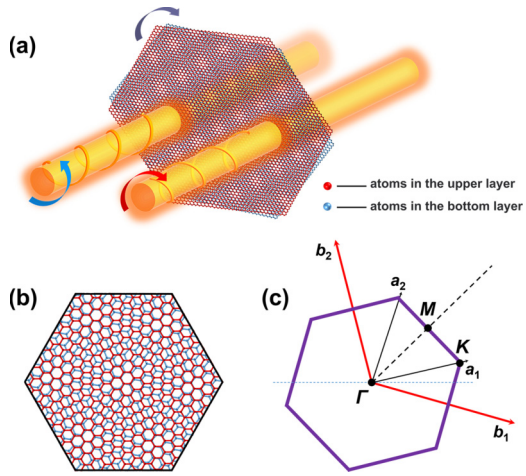

FIG. 1. Diagram of TBG. (a) The schematics of optical absorption for either the right and the left circularly polarized light passing through the chiral TBG. (b) The moiré pattern of the TBG lattice. (c) The first Brillouin zone of TBG, where a_1, a_2 are the basis vectors in real space, and b_1 and b_2 are the reciprocal lattice vectors. Γ, K, and M are high-symmetry points.

absorption in the low-frequency domain either by changing the twisting angle or by an interlayer bias. The theory is also applicable to other twisted bilayer structures.

The paper is organized as follows. In Sec. II, the detailed absorption theory dealing with TBG is presented. We discuss the lattice model and its energy band structure, taking the spin-orbit coupling (SOC) into account. Also, the absorption formula beyond the common linear absorption with more sophisticated light-electron interactions is considered. Section III is about the numerical results and discussions, including the absorption spectra for both linear and circular polarizations, and the dependence on the twisted angle and the interlayer bias. A conclusion is drawn in Sec. IV.

II. METHODS

The TBG is a two-layer structure, with the upper layer rotated at an angle θ ($-\pi/6 < \theta < \pi/6$) in an anticlockwise direction (right-handed helical structure), using one of the aligned carbon atoms as the center point. The resulting moiré pattern also possesses a hexagonal lattice, but with a larger unit cell. When θ is positive or negative, a different chirality is introduced. For a circularly polarized light incident from the upper layer to the lower layer, the chiral structure exhibits different responses to left and right circularly polarized light, as illustrated in Fig. 1(a). To reveal the effect of chirality, a more sophisticated theory beyond traditional absorption theory is required.

Under the perturbation of the electromagnetic field, the Hamiltonian of the irradiated system reads

$$\hat{H} = \hat{H}_0 + \hat{H}', \tag{1}$$

$$\hat{H}_0 = \left[\frac{\hat{\mathbf{p}}^2}{2m} + V(\hat{\mathbf{r}}) + H_{\mathrm{SOC}}\right], \tag{2}$$

$$\hat{H}' = \left[\frac{e}{2m}(\hat{\mathbf{p}}\cdot\mathbf{A} + \mathbf{A}\cdot\hat{\mathbf{p}}) - e\phi + \frac{e}{m}\hat{\mathbf{S}}\cdot\mathbf{B}\right], \tag{3}$$

where $-e, m, \mathbf{S}$ are the charge, the mass, and the spin of an electron, respectively. ϕ is the electric potential of the electron. $\mathbf{A}$ and $\mathbf{B}$ denote the magnetic potential and the magnetic flux density of the accompanied electromagnetic field of the incident light, respectively. The electric field intensity $\mathbf{E}$ can also be obtained from them. H_{SOC} is the spin-orbit coupling term that has garnered significant attention and research due to its ability to eliminate the spin degeneracy of electronic bands and induce a gap opening in few-layer graphene and other two-dimensional (2D) materials [33–37]. Furthermore, the magnetic component of light mainly interacts with the spin magnetic moment. Thus, considering spin is a reasonable approach. The perpendicular incidence of light breaks the inversion symmetry of the system, resulting in the presence of extrinsic spin-orbit coupling, known as the Rashba term.

A. Band structure

The Hamiltonian of H_0 in Eq. (3) can be expressed as

$$\hat{H}_0 = \left[\sum_{k,n} t(\mathbf{d}_{kn}) c_k^\dagger c_n + \mathrm{H.c.}\right] + \sum_m \epsilon_m c_m^\dagger c_m + \hat{H}_{\mathrm{SOC}}, \tag{4}$$

where c ($c^\dagger$) is the annihilation (creation) operator and ϵ_m represents the on-site energy at site m. The first term in the Hamiltonian is the kinetic energy, the second term is the potential energy, and the third term represents the spin-orbit coupling.

The hopping parameter t is determined by the relative position vector from the initial atom site n to the final atom site k, $\mathbf{d}_{kn} = \mathbf{d}_k - \mathbf{d}_n$. Considering both the interlayer and intralayer contributions, the hopping intensity of an electrons is [23,38–41]

$$\begin{aligned} t(\mathbf{d}_{kn}) &= V_{pp\pi}\left[1 - \left(\frac{\mathbf{d}_{kn}\cdot\mathbf{e}_z}{d_{kn}}\right)^2\right] + V_{pp\sigma}\left(\frac{\mathbf{d}_{kn}\cdot\mathbf{e}_z}{d_{kn}}\right)^2, \\ V_{pp\pi} &= V_{pp\pi}^0 \exp\left(-\frac{d_{kn} - a_{\mathrm{CC}}}{\delta_0}\right), \\ V_{pp\sigma} &= V_{pp\sigma}^0 \exp\left(-\frac{d_{kn} - d_0}{\delta_0}\right), \end{aligned} \tag{5}$$

where a_{CC} is the length of the carbon-carbon bond in graphene, and $\delta_0 = 0.045$ nm represents the decay length. The spacing between the graphene layers d_0 is 0.335 nm. Here, $V_{pp\pi}^0 = -2.7$ eV, $V_{pp\sigma}^0 = 0.48$ eV are the interlayer and intralayer nearest-neighbor hopping intensities, respectively.

In the paper, we only consider the commensurate case, i.e., a strict supercell formed when certain new pairs of carbon atoms are aligned. In this case the twisted angle (commensurate angles) takes a series of discrete values θ satisfying

$$\theta = 2\arctan\left[\frac{\sqrt{3}(a-b)}{3(a+b)}\right], \tag{6}$$

where a and b are prime and $a > b$. This is determined by the geometrical characteristics of the bilayer honeycomb lattice. For an example, the lattice diagram in the case of $a = 5, b = 4$ is shown in Fig. 1(b) where the twisted angle is 7.34°.

In order to demonstrate the chirality of the TBG irradiated by a perpendicularly incident light, it makes sense to consider

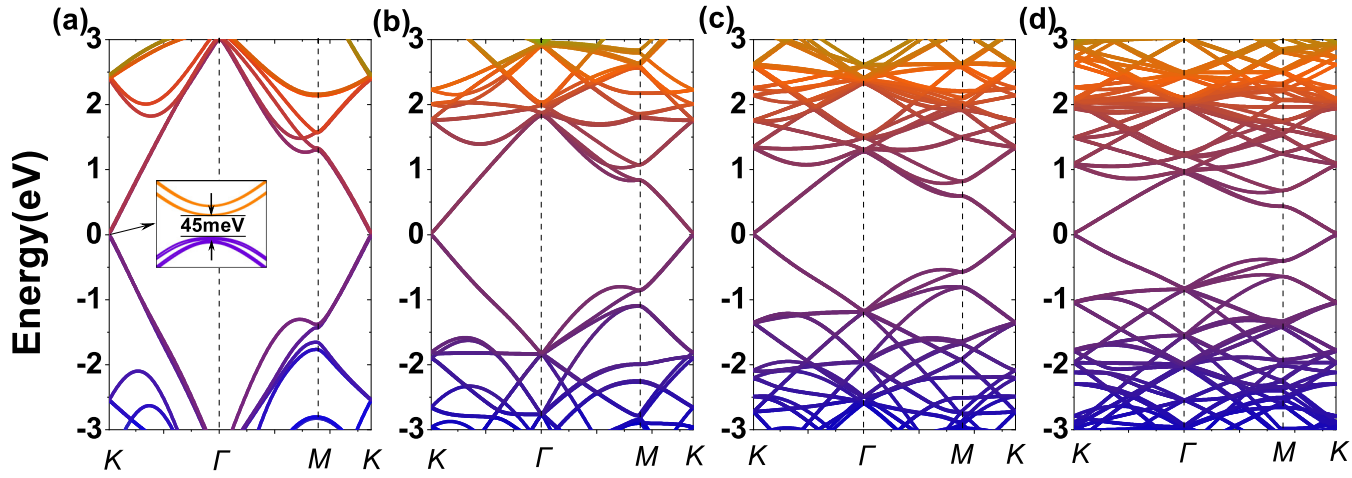

FIG. 2. The energy bands of the TBG system in a series of twisted angles. (a) 21.8°. (b) 13.17°. (c) 9.43°. (d) 7.34°.

the intrinsic spin-orbit coupling, the Rashba term, and the interlayer Rashba term [33–35,42]. The spin-orbit coupling term can be expressed as

$$\hat{H}_{\mathrm{SOC}} = it_{\mathrm{ISO}} \sum_{\langle\langle i,j\rangle\rangle} v_{ij} c_i^{\dagger} \sigma_z c_j + it_R \sum_{\langle i,j\rangle} c_i^{\dagger} (\sigma \times \hat{\mathbf{d}}_{ij}) \cdot \hat{\mathbf{e}}_z c_j - it_R^{\perp} \sum_i c_{i,1}^{\dagger} (\sigma \times \hat{\mathbf{e}}_z) \cdot \hat{\mathbf{e}}_{\parallel} c_{i,2} + \mathrm{H.c.}, \tag{7}$$

where $t_{\mathrm{ISO}} = 0.0016 V_{pp\pi}^0 \approx 4.32$ meV, $t_R = 0.004 V_{pp\pi}^0 \approx 10.8$ meV, $t_R^{\perp} = 0.001 V_{pp\pi}^0 \approx 2.7$ meV are the coupling coefficients of the intrinsic spin-orbit coupling, the intralayer Rashba coupling, and the interlayer Rashba coupling, respectively [43–46]. σ is the Pauli matrix. The intrinsic spin-orbit coupling represents the next-nearest-neighbor (NNN) hopping. When NNN hopping is anticlockwise, v_{ij} is $+1$, and when the NNN hopping is clockwise, v_{ij} is -1. The Rashba coupling is the nearest-neighbor hopping. $\hat{\mathbf{d}}_{ij}$ is the unit vector connecting the two nearest-neighbor sites i and j. $\hat{\mathbf{e}}_{\parallel}$ is the unit vector of the in-plane component of the electric field, which causes the interlayer Rashba coupling. Its direction has no effect on the results so it can be taken as (1,0,0).

The energy band structure of TBG in this situation can be obtained, as shown in Fig. 2, where the commensurate angle takes four values: 21.8°, 13.17°, 9.43°, and 7.34°. It can be seen that decreasing the twisted angles narrows the conduction-valence spacing and also flattens the energy bands over a large range of $\mathbf{k}$. In the absence of spin-orbit coupling, there would be a Dirac cone at the K point. However, when SOC is introduced, there appears to be a band gap at the K point, with its value determined by the strength of SOC.

B. Optical absorption

The incident light propagating in the z direction reads

$$\mathbf{E} = E_0 e^{ikz} e^{i\omega t} \mathbf{e}_E, \tag{8}$$

$$\mathbf{B} = \frac{E_0}{c} e^{ikz} e^{i\omega t} \mathbf{e}_B, \tag{9}$$

where k is the wave number and ω is the angular frequency. E_0 is the amplitude of the electric field. The sign $+$ of the exponent part of the spatial phase term e^{ikz} means that the direction of light propagation is negative towards the z axis. $\mathbf{e}_E$ and $\mathbf{e}_B$ are unit vectors in the direction of the electric field and magnetic induction intensity, satisfying the relationship $\mathbf{e_B} = \hat{\mathbf{e}}_z \times \mathbf{e_E}$. Choosing the gauge to let $\phi = 0$, and so

$$\mathbf{A} = -\frac{E_0}{i\omega} e^{ikz} e^{i\omega t} \mathbf{e}_E. \tag{10}$$

Then applying the condition that $\mathbf{p}$ and $\mathbf{A}$ is commutative, the perturbation Hamiltonian can be expanded according to the order of z as

$$\begin{aligned} \hat{H}' &= \hat{H}_1' + \hat{H}_2' \\ &= -\frac{q}{m}\left(-\frac{E_0}{i\omega} e^{ikz}\right)(\hat{\mathbf{p}} \cdot \mathbf{e}_E) - \frac{q}{m} \hat{\mathbf{S}} \cdot \mathbf{e}_B \left(\frac{E_0}{c} e^{ikz}\right) \\ &= \frac{qE_0}{im\omega}[(\hat{\mathbf{p}} \cdot \mathbf{e}_E)] + \frac{qE_0}{im\omega}\left[ik\hat{z}(\hat{\mathbf{p}} \cdot \mathbf{e}_E) + \frac{\omega}{ic}(\hat{\mathbf{S}} \cdot \mathbf{e}_B)\right] \\ &\quad + \cdots, \end{aligned} \tag{11}$$

where $\hat{H}_{1(2)}'$ means the first- (second-) order perturbation Hamiltonian and $\cdots$ represents high-order terms. Note that the term $e^{i\omega t}$ has been dropped off temporally.

Due to the short interlayer distance of TBG, high-order terms in the above equation can be neglected, and the limit $z \to 0$ can be applied to the calculation. In other words, only the first-order term (the electric dipole) and the second-order term (including the magnetic dipole and the electric quadrupole) are considered.

It can be verified that the first-order perturbation is insensitive to the polarization of circularly polarized light. Therefore, in order to observe the polarization dependence of circularly polarized light, the second-order perturbation is necessary.

The eigenstate $|\phi_n\rangle$ would be affected by the perturbation from the incident light, and its component in the k state is

$$c_k(t) = \frac{1}{i\hbar} \int_0^t H_{kn}'(\tau) e^{-i\omega_{kn}\tau} d\tau, \tag{12}$$

where $H'_{kn}(t) = \langle\phi_k|H'(t)|\phi_n\rangle$, $\omega_{kn} = \frac{1}{\hbar}(E_k - E_n)$. The transition probability between eigenstates n and k is then

$$P_{n\to k} \propto \frac{d}{dt}\left|\int_0^t H'_{kn}(\tau)d\tau e^{-i\omega_{kn}\tau}\right|^2. \quad (13)$$

By assuming the perturbation is $H'(t) = H'e^{i\omega t}$ where ω is the frequency of incident light, then c_k becomes

$$c_k(t) = \frac{H'_{kn}}{i\hbar}\int_0^t e^{i\omega\tau}e^{-i\omega_{kn}\tau}d\tau = \frac{H'_{kn}}{i\hbar}\left[\frac{e^{i(\omega-\omega_{kn})t}-1}{i(\omega-\omega_{kn})}\right]. \quad (14)$$

Using the formula of the δ function $\delta(x) = \lim_{t\to\infty}\frac{\sin^2(xt)}{2\pi x^2 t}$ and ignoring higher-order quantities, the transition probability becomes

$$P_{n\to k} = \frac{2\pi}{\hbar}|H'_{kn}|^2\delta(E_k - E_n - \hbar\omega). \quad (15)$$

Finally, the optical absorption corresponds to the transition rate per unit time,

$$A(\omega) \propto |H'_{kn}|^2[\delta(E_k - E_n - \hbar\omega)], \quad (16)$$

where the δ function represents the optical transition condition. This formula has the form of standard optical absorption, however, the detailed contents included in $H'(t)$ as given by Eq. (11) would produce different responses of the chiral system to the circularly polarized light.

III. RESULTS AND DISCUSSION

In this section, we will discuss the results of optical absorption in TBG under different conditions, including linear polarization of incident light, twisted angles, and interlayer electric bias. Finally, the case of circular polarization of light will be explored, which is related to the chirality of TBG. Without loss of generality, we will consider a specific system where $a = b + 1$ for twisted bilayer graphene.

A. Linear polarization

For absorption on linearly polarized light, first-order perturbation is enough, i.e., we can neglect the second perturbation term about the magnetic field in Eq. (3). In this case, the absorption formula can be obtained as

$$A(\omega, \mathbf{k}) \propto \sum_{n,k}\frac{1}{\omega_{kn}^2}|\mathbf{E}\cdot\langle\psi_k(\mathbf{k})|(\nabla_{\mathbf{k}}H_0(\mathbf{k}))|\psi_n(\mathbf{k})\rangle|^2 \times \mathrm{Im}\frac{f(E_k(\mathbf{k})) - f(E_n(\mathbf{k}))}{(E_k - E_n) - \omega - i\gamma}, \quad (17)$$

where the initial and final states are located in the valence and the conduction bands, respectively. The Fermi surface is set to zero. $\mathbf{E}$ is the electric field vector of linearly polarized light. The function f in the last term is the Fermi-Dirac distribution. γ is a broadening factor and takes a value of 0.03 eV. To calculate the overall absorption of light by TBG, this result should be integrated over the first Brillouin zone. However, the area around K in the reciprocal space makes the main contribution especially for low-energy absorption.

We choose TBG with a twisted angle of 21.8° to calculate the dependence of the light absorption at 514 nm on the polarization direction. In Fig. 3, the light absorption of TBG twisted by 21.8° is drawn for different polarization vectors of incident light E. It is obvious that the absorption has a certain polarization dependence, featuring the anisotropy of the TBG.

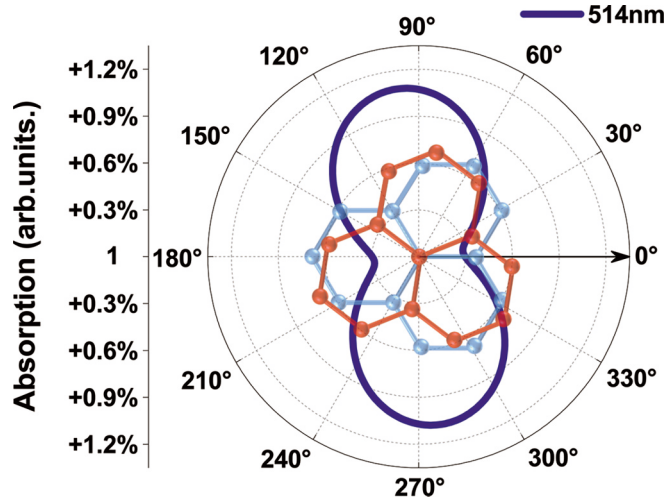

FIG. 3. Polar diagram of light absorption of 21.8° TBG for 514 nm light. The angle is the polarization angle, whose zero point is defined as shown of the lattice in the background.

B. Twisted angle

We here check the dependence of optical absorption of TBG on the twisted angle for a fixed polarization direction ($\theta/2$). The twisted angle θ is set to three commensurate angles, 21.8°, 13.17°, and 9.43°, respectively. The absorption mainly happens in the low-energy domain, an order of magnitude larger than that in the high-energy range, and is immune to the twisted angle, as shown in the left-hand panel of Fig. 4. In the high-energy situation, as plotted in the right-hand panel of Fig. 4, the absorption is relatively weak, but the first one (at 2–3 eV) experiences an outstanding redshift with the angle decreasing and the second one (at 5 eV) a small blueshift, which is consistent with the previous experimental [22] and theoretical works [23,28]. The results are consistent with the evolution of the energy band structure: low-energy absorption occurs near the band gap at the K point, which possesses a heavy optical transition and whose energy scale is mainly

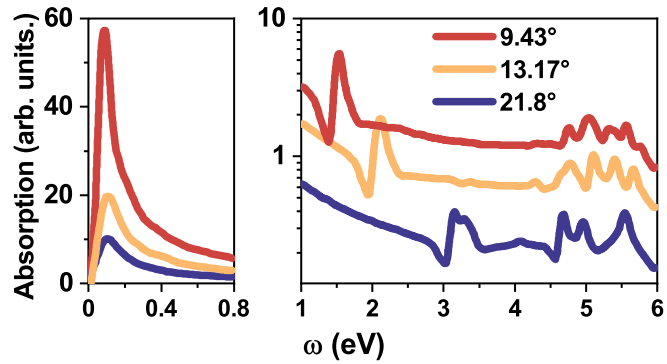

FIG. 4. Optical absorption of TBG at different twisted angles at the higher- and lower-energy range of light.

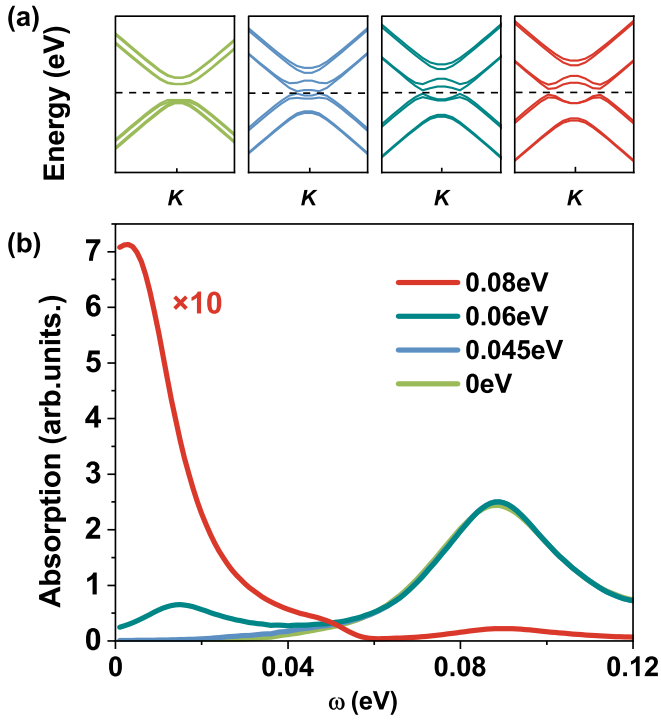

FIG. 5. (a) The energy band structure around the K point and (b) the optical absorption in the low-energy domain of 21.8° TBG subjected to different interlayer electric fields.

determined by the SOC, while high-energy absorption is caused by the narrowed band gap as a whole when the twisted angle decreases. Note that the vertical axis in the right-hand panel of Fig. 4 is exponential, which means there exists a large difference in optical absorption for these three twisted angles.

C. Interlayer bias

When a perpendicular electric field is applied to TBG, a potential difference arises between the two layers, which modifies the on-site energy terms in the Hamiltonian of Eq. (4). Consequently, the valence and conduction are deformed into Mexican hats near the K point and anticrossing points with a band gap of about 20 meV form rings. For instance, Fig. 5(a) illustrates the evolution of the energy band structure for 21.8° TBG. The conduction and valence bands contact and then progressively form the anticrossing structure as the bias increases from 0 to 0.08 eV. In these bands, the increase in the radius of the rings formed by the anticrossing points makes the probability of optical transitions surge near 0 eV. Numerical calculations also support a significant enhancement in the absorption of low-frequency light. As depicted in Fig. 5(b), the corresponding absorption in the low-energy domain emerges as the band gap is reduced by the interlayer bias, and starts to increase significantly once the bias is greater than the threshold value of the band-gap closure (0.045 eV).

D. Circular polarization

When the incident light is circularly polarized, it is expected that the chirality of TBG can be observed. However, the first-order perturbation applied in Eq. (17) cannot differentiate the left and the right circular polarization cases. To distinguish them, the second-order perturbation induced by the light field needs to be considered, which includes contributions from both electric quadrupole and magnetic dipole terms. Taking SOC into account, the absorption can be expressed as

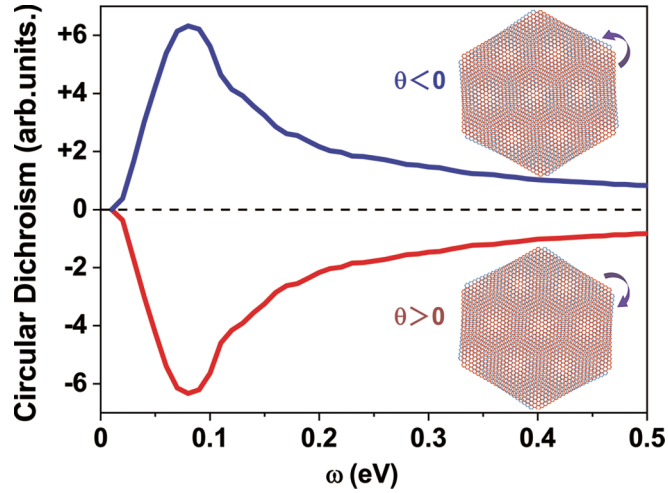

FIG. 6. CD spectrum of TBG. The insets are diagrams of the twisting direction of TBG. θ represents the twisted angle of the upper layer relative to the bottom layer along the direction of incident light.

$$A_{\pm}(\omega,\mathbf{k}) \propto \sum_{n,k} \left(H'^{*}_{1\pm}H'_{2\pm} + H'^{*}_{2\pm}H'_{1\pm}\right) \times \mathrm{Im}\frac{f(E_k(\mathbf{k})) - f(E_n(\mathbf{k}))}{(E_k - E_n) - \omega - i\gamma}, \tag{18}$$

$$H'_{1\pm} = \frac{1}{\omega_{kn}}\langle\psi_k|(\hat{p}_x \pm i\hat{p}_y)|\psi_n\rangle,$$

$$H'_{2\pm} = \frac{1}{c}\langle\psi_k|i(\hat{z}\hat{p}_x \pm i\hat{z}\hat{p}_y \pm i\hat{s}_x - \hat{s}_y)|\psi_n\rangle, \tag{19}$$

where the sign + (−) represents the right-handed (left-handed) circularly polarized case. As the SOC would produce a band gap as given in Fig. 2, there appears to be a strong optical absorption on the energy scale of the band gap, i.e., 0000.2 eV in our parameters. The chiral circular dichroism (CD) spectrum, defined as $A_- - A_+$, can be used to distinguish the chirality of the TBG. The CD spectrum of 21.8° TBG, calculated numerically based on our theory, is presented in Fig. 6, which exhibits distinct differences between left-handed and right-handed chiral TBG. It has been checked that changing the direction of the incident light ($\hat{z} \to -\hat{z}$) can also produce the same CD spectrum. This indicates that the CD spectrum is independent of the specific direction of the incident light and remains consistent for a given chiral configuration. Therefore, the theory, taking advantages of the spin-orbit coupling and high-order perturbations, provides an effective method to detect the chirality of TBG.

IV. CONCLUSION

We investigate the optical absorption in TBG, developing the absorption theory with both the fine band structure and

the high-order light-TBG interaction considered. Under the theory, the numerical calculations on the absorption are conducted to show the dependence of absorption on the light polarization, the twisted angle, and the vertical electric field, respectively. The results show that (a) the absorption experiences a redshift in the high-frequency range and is enhanced significantly by decreasing the twisted angle; (b) the absorption strength can be significantly improved by increasing interlayer bias; (c) the absorption for linearly polarized light demonstrates anisotropy of TBG; and (d) the absorption for circularly polarized light manifests the chirality of TGB. We conclude that the absorption theory could be a valid method to detect the structural characteristics of TBG, especially the chirality.

[1] Z. Han, F. Wang, J. Sun, X. Wang, and Z. Tang, Adv. Mater. **35**, 2206141 (2022).

[2] E. Y. Andrei and A. H. MacDonald, Nat. Mater. **19**, 1265 (2020).

[3] G. Dai, X. Chen, Y. Jin, and J. Wang, Molecules **27**, 6525 (2022).

[4] S. Carr, D. Massatt, S. Fang, P. Cazeaux, M. Luskin, and E. Kaxiras, Phys. Rev. B **95**, 075420 (2017).

[5] J. Wang, X. Mu, L. Wang, and M. Sun, Mater. Today Phys. **9**, 100099 (2019).

[6] J. Song and M. Sun, J. Mater. Chem. A **11**, 13519 (2023).

[7] X. Mu and M. Sun, Mater. Today Phys. **14**, 100222 (2020).

[8] J. González and T. Stauber, Phys. Rev. Lett. **124**, 186801 (2020).

[9] Y. Cao, V. Fatemi, S. Fang, K. Watanabe, T. Taniguchi, E. Kaxiras, and P. Jarillo-Herrero, Nature (London) **556**, 43 (2018).

[10] P. Wilhelm, T. C. Lang, and A. M. Läuchli, Phys. Rev. B **103**, 125406 (2021).

[11] X. Lu, P. Stepanov, W. Yang, M. Xie, M. A. Aamir, I. Das, C. Urgell, K. Watanabe, T. Taniguchi, G. Zhang *et al.*, Nature (London) **574**, 653 (2019).

[12] N. R. Chebrolu, B. L. Chittari, and J. Jung, Phys. Rev. B **99**, 235417 (2019).

[13] Z. Ma, S. Li, Y. Zheng, M. Xiao, H. Jiang, J. Gao, and X. Xie, Sci. Bull. **66**, 18 (2021).

[14] Y. Park, B. L. Chittari, and J. Jung, Phys. Rev. B **102**, 035411 (2020).

[15] P. J. Ledwith, A. Vishwanath, and E. Khalaf, Phys. Rev. Lett. **128**, 176404 (2022).

[16] R. Bistritzer and A. H. MacDonald, Proc. Natl. Acad. Sci. USA **108**, 12233 (2011).

[17] M. Reist, P.-A. Carrupt, E. Francotte, and B. Testa, Chem. Res. Toxicol. **11**, 1521 (1998).

[18] S. Yoo and Q. H. Park, Nanophotonics **8**, 249 (2019).

[19] K. Ariga, G. J. Richards, S. Ishihara, H. Izawa, and J. P. Hill, Sensors **10**, 6796 (2010).

[20] W. Wen and Q.-X. Guo, Synthesis **55**, 719 (2023).

[21] Y. Lu, Z. F. Cui, Z. Pan, C. H. Chang, and H. S. Zong, Phys. Rev. D **93**, 074037 (2016).

[22] C. J. Kim. A. Sánchez-Castillo, Z. Ziegler, Y. Ogawa, C. Noguez, and J. Park, Nat. Nanotechnol. **11**, 520 (2016).

[23] P. Moon and M. Koshino, Phys. Rev. B **87**, 205404 (2013).

[24] E. J. Nicol and J. P. Carbotte, Phys. Rev. B **77**, 155409 (2008).

[25] P. Moon, Y. W. Son, and M. Koshino, Phys. Rev. B **90**, 155427 (2014).

[26] K. Yu, N. Van Luan, T. Kim, J. Jeon, J. Kim, P. Moon, Y. H. Lee, and E. J. Choi, Phys. Rev. B **99**, 241405(R) (2019).

[27] C. J. Tabert and E. J. Nicol, Phys. Rev. B **86**, 075439 (2012).

[28] E. S. Morell, L. Chico, and L. Brey, 2D Mater. **4**, 035015 (2017).

[29] T. Stauber, T. Low, and G. Gómez-Santos, Phys. Rev. Lett. **120**, 046801 (2018).

[30] Z. Addison, J. Park, and E. J. Mele, Phys. Rev. B **100**, 125418 (2019).

[31] A. V. Poshakinskiy, D. R. Kazanov, T. V. Shubina, and S. A. Tarasenko, Nanophotonics **7**, 753 (2018).

[32] S. T. Ho and V. N. Do, Phys. Rev. B **107**, 195141 (2023).

[33] C. L. Kane and E. J. Mele, Phys. Rev. Lett. **95**, 146802 (2005).

[34] C. L. Kane and E. J. Mele, Phys. Rev. Lett. **95**, 226801 (2005).

[35] R. van Gelderen and C. M. Smith, Phys. Rev. B **81**, 125435 (2010).

[36] J. J. chen, K. Wu, W. Hu, and J. L. Yang, J. Phys. Chem. Lett. **12**, 12256 (2021).

[37] M. F. Sahdan and Y. Darma, AIP Conf. Proc. **1589**, 253 (2014).

[38] M. Mirzakhani, F. M. Peeters, and M. Zarenia, Phys. Rev. B **101**, 075413 (2020).

[39] T. Nakanishi and T. Ando, J. Phys. Soc. Jpn. **70**, 1647 (2001).

[40] G. Trambly de Laissardière, D. Mayou, and L. Magaud, Nano Lett. **10**, 804 (2010).

[41] S. Uryu, Phys. Rev. B **69**, 075402 (2004).

[42] G. Bihlmayer, O. Rader, and R. Winkler, New J. Phys. **17**, 050202 (2015).

[43] S. Konschuh, M. Gmitra, and J. Fabian, Phys. Rev. B **82**, 245412 (2010).

[44] C. Weeks, J. Hu, J. Alicea, M. Franz, and R. Wu, Phys. Rev. X **1**, 021001 (2011).

[45] H. Jiang, Z. Qiao, H. Liu, J. Shi, and Q. Niu, Phys. Rev. Lett. **109**, 116803 (2012).

[46] H. Min, J. E. Hill, N. A. Sinitsyn, B. R. Sahu, L. Kleinman, and A. H. MacDonald, Phys. Rev. B **74**, 165310 (2006).